Journal of Alloys and Compounds 773 (2019) 299–304

Contents lists available at ScienceDirect

Journal of Alloys and Compounds

journal homepage: http://www.elsevier.com/locate/jalcom

Excellent gas sensing of hierarchical urchin-shaped Zn doped cadmium sulfide

Zhangshu Huang, Dongdong Wei, Tianshuang Wang, Wenhao Jiang, Fangmeng Liu, Xiaohong Chuai*, Xishuang Liang, Yuan Gao, Peng Sun, Xu Yan, Jie Zheng, Hongwei Song, Geyu Lu

State Key Laboratory on Integrated Optoelectronics, College of Electronic Science and Engineering, Jilin University, 2699 Qianjin Street, Changchun, 130012, People's Republic of China

A R T I C L E I N F O

Article history:
Received 10 April 2018
Received in revised form
30 August 2018
Accepted 17 September 2018
Available online 18 September 2018

Keywords:
Zn doped CdS
Hydrothermal
Hierarchical structures
Gas sensor

A B S T R A C T

Urchin-like hierarchical Zn doped CdS powders were successfully synthesized via simple one-pot hydrothermal process. Their SEM and TEM images indicated that the hierarchical structure were assembled by single crystal nanorods with the hexagonal wurtzite phase. EDS element mapping verified that Zn ions were homogeneously distributed among the hierarchical microstructure. The performances of gas sensors based on pure and Zn doped CdS were measured and compared. The results indicated that Zn doping could enhance their responses to some volatile organic compounds and improve its selectivity to ethanol and toluene as well. The possible reasons for this enhancement were investigated. In addition, the sensor based on Zn doped CdS exhibited the ultrafast response and recovery to ethanol ($\tau_{response} < 1$, $\tau_{recovery} = 8s$), indicating that the Zn doped CdS could be a promising gas sensing candidate for online monitoring of ethanol.

1. Introduction

Gas sensors are playing more and more vital roles on the air-quality monitoring and medical diagnosis. Chemiresistive gas sensors, based on semiconductor oxides, are widely investigated in the past few decades because of their superior gas sensing properties, low cost and ease for operation [1–7]. Gas sensing relies on the surface chemical reaction between target gas and chemical absorbed oxygen on the surface of sensing material. The microstructure of sensing materials embody their comprehensive properties related with surface activity, gas transportation etc. Therefore, their sensing properties can be further adjusted and optimized by controlling their microstructure [8,9]. Compared with low dimension nanomaterials such as one-dimensional(1D) and two-dimensional(2D) building blocks, three-dimensional(3D) hierarchical sensing materials may present more fascinating sensing properties owing to large surface area, favorable gas diffusion and well-defined morphology. Consequently, simple and efficient ways to synthesize the 3D hierarchical nanomaterials are highly expected to explore gas sensor with excellent performance. For the resistance-type gas sensor, semiconductor oxides, such as ZnO [10–12], α-Fe_2O_3 [13], In_2O_3 [14,15], WO_3 [16–19], SnO_2 [20,21], are dominantly be studied. However, research reports on the metal chalcogenides in the field of gas sensor have rarely been reported in the past years [22–24], in spite of their extraordinary optoelectronic properties in visible-light detector, sensors, waveguide photodetectors, lasers, field-effect transistors, solar cell and photocatalysis etc. Ruan et al. [25] reported that Zn1-xCdxS nanowire had response of 12 toward 50 ppm ethanol. Ma et al. [26] verified that CdS microparticle could response to 30 ppm NO with sensitivity of 65.8 at the operating temperature of 180 °C. Thus it can be seen that CdS is a potential good sensing material. Its sensing performance is worthy of further investigation. In order to improve the sensing performance, several effective methods such as doping, noble metal loading and construction of heterojunction have been adopted. Doping is a simple and effective method. Zn^{2+} ion was selected to be doped in the CdS because of the similar crystal structure of ZnS and CdS. In our work, unique urchin-like hierarchical CdS assembled by a large number of nanorods firstly prepared by one-step hydrothermal route. The gas sensors based on the as-synthesized CdS were fabricated and their gas sensing performances were investigated and compared. The results showed

* Corresponding author.
E-mail address: xhchuai@jlu.edu.cn (X. Chuai).

https://doi.org/10.1016/j.jallcom.2018.09.219

that Zn doped CdS exhibited high response sensitivity and fast response-recovery property to ethanol at 225 °C.

2. Experimental

2.1. Synthesis of urchin-like hierarchical CdS

All the reagents in the experiment were purchased from Beijing Chemical Reagent and used as received without further purification. 0.1M cadmium nitrate and thiourea solutions were prepared for the cadmium and sulfide precursors, respectively. In a typical experiment, 0.05 g ZnO was added in 40 ml mixture of deionized water and ethylenediamine (1:2 v/v) with vigorous stirring till it was solved completely. Then appropriate amounts of cadmium nitrate and thiourea solution (1:1 v/v) were mixed with the above solution. Being stirred for 20 min, the mixed solution was transferred into a 45 ml Teflon-lined stainless autoclave and maintained at 180 °C for 12 h. On cooling down, the precipitates were collected by centrifugation, repeatedly washed with distilled water and absolute ethanol for several times, and dried at 80 °C in air. Different amounts of cadmium nitrate (0.25 ml, 0.50 ml, 0.75 ml) were added in the hydrothermal procedure, and the corresponding products were labeled as S1, S2 and S3, respectively. They were classified as Zn doped CdS. If the above hydrothermal process was repeated with the fixed 0.25 ml cadmium nitrate and no addition of ZnO, the obtained sample was labeled as pure CdS.

2.2. Characterization

The phase structures of the as-synthesized products were analyzed by a Rigaku TTRIII X-ray diffractometer with Cu Kα_1 radiation ($\lambda = 1.5406$A). The surface morphology and microstructure of the prepared samples were observed by field emission scanning electron microscope (SEM, JEOL JSM-7500F) at an acceleration voltage of 15 kV and transmission electron microscopy (TEM, JEOL JEM-3010) at 200 kV. The energy dispersive X-ray spectroscopic (EDS) elemental mappings were investigated by the TEM attachment.

2.3. Fabrication and measurement of gas sensor

The gas sensor was fabricated as follows: the as-synthesized powder was first dispersed in deionized water in volume ratio of 5:1 to form homogeneous slurry. Subsequently, it was coated onto an alumina tube (4 mm in length, 1.2 mm in external diameter, and 0.8 mm in internal diameter, attached with a pair of gold electrodes) with a brush to form a thick sensing film. Being baked for 10 min under an infrared lamp, it was sintered at 300 °C for 2 h to improve its thermal stability. Then a Ni-Cr alloy coil was inserted into the alumina tube as a heater in order to control the operating temperature of the sensor. A RQ-2 series Intelligent Test Meter (made in China) was applied to investigate the sensing performance of the sensor. The measurement was carried out by a static process, that is to say, the sensor was alternately placed into the test chambers full of air and a kind of target gas with certain concentration and the corresponding resistance (R_a or R_g) was measured respectively. The resistance ratio of R_g/R_a in an oxidative target gas was defined as response value. On the contrary, in a reductive gas, the response was expressed as R_a/R_g.

3. Results and discussion

3.1. Structural and morphological characteristics

Fig. 1a shows the X-ray diffraction (XRD) patterns of pure and Zn

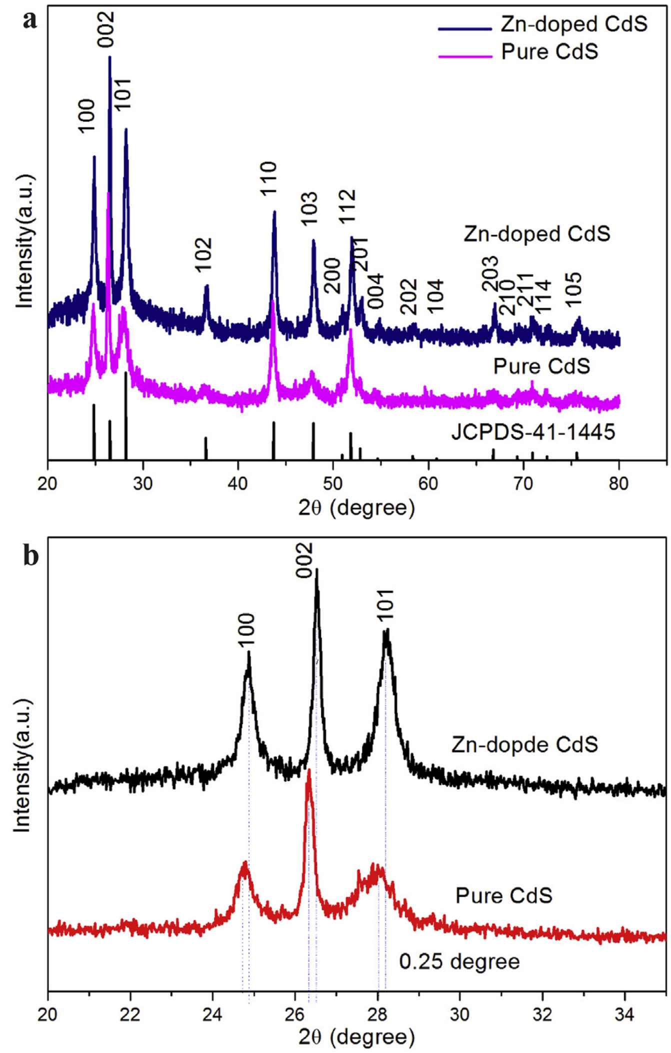

Fig. 1. a XRD patterns of pure and Zn doped CdS (S1)samples. b Enlarged XRD patterns between the range of 20 and 35 degree.

doped CdS (S1) products. As seen in Fig. 1a, all the diffraction peaks can be indexed to those of hexagonal wurtzite CdS (JCPDS card No. 89-2944) (a = 4.14 Å, c = 6.715 Å). No extra diffraction peaks are observed. To further differentiate the corresponding peak positions for pure and Zn doped CdS, their enlarged diffraction patterns in the range of 20–35° (shown in Fig. 1b) are evaluated. Compared with pure CdS, the peak positions for Zn doped CdS shift slightly towards large diffraction angle, confirming that Zn^{2+} ions with smaller ion radii than Cd^{2+} are doped into the CdS lattice (R_{Zn}:74pm, R_{Cd}:95pm). The morphologies and microstructures of the as-prepared products were illustrated by FESEM photographs (shown in Fig. 2). It is observed that both Zn-doped and pure CdS exhibit urchin-like hierarchical structure, with the former having more regular and homogenous structure. The urchin-like hierarchical structures are assembled by a lot of nanorods with the diameter between 30 and 50 nm and length between 0.5 and 0.8 μm. Moreover, HRTEM and TEM elemental mapping were employed to further analyze the lattice structure and the elemental distribution of the as-prepared Zn doped CdS hierarchical structure. Fig. 3a, b, f display the TEM imagines of Zn doped CdS microstructure, showing that urchin-like hierarchical structure consists of numerous nanorods. The clear lattice fringes in a single nanorod

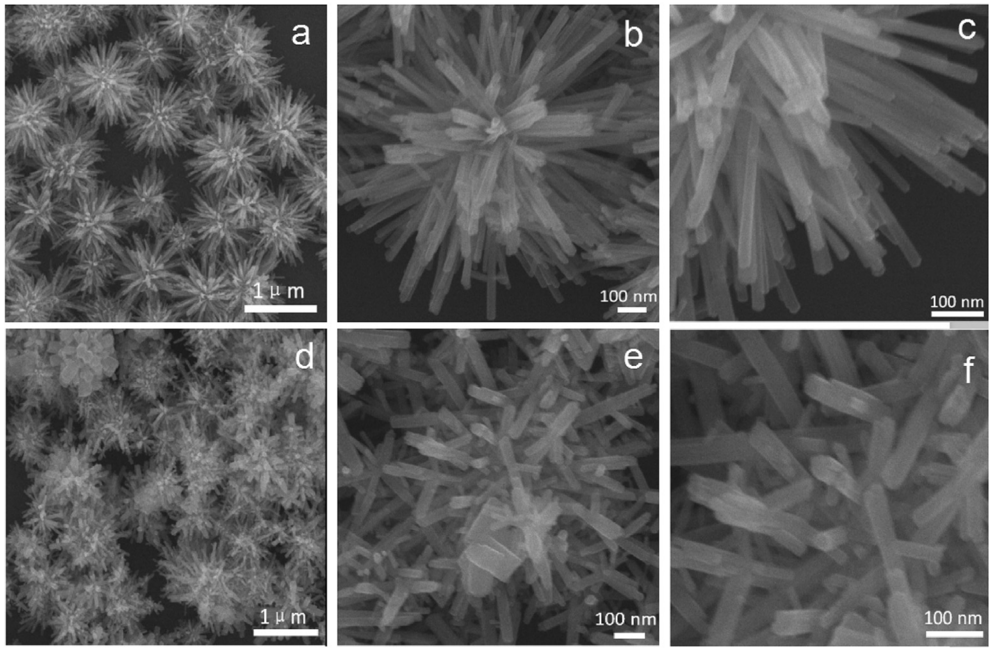

Fig. 2. SEM images of CdS: (a, b, c) Zn doped CdS (S1), (d, e, f) pure CdS.

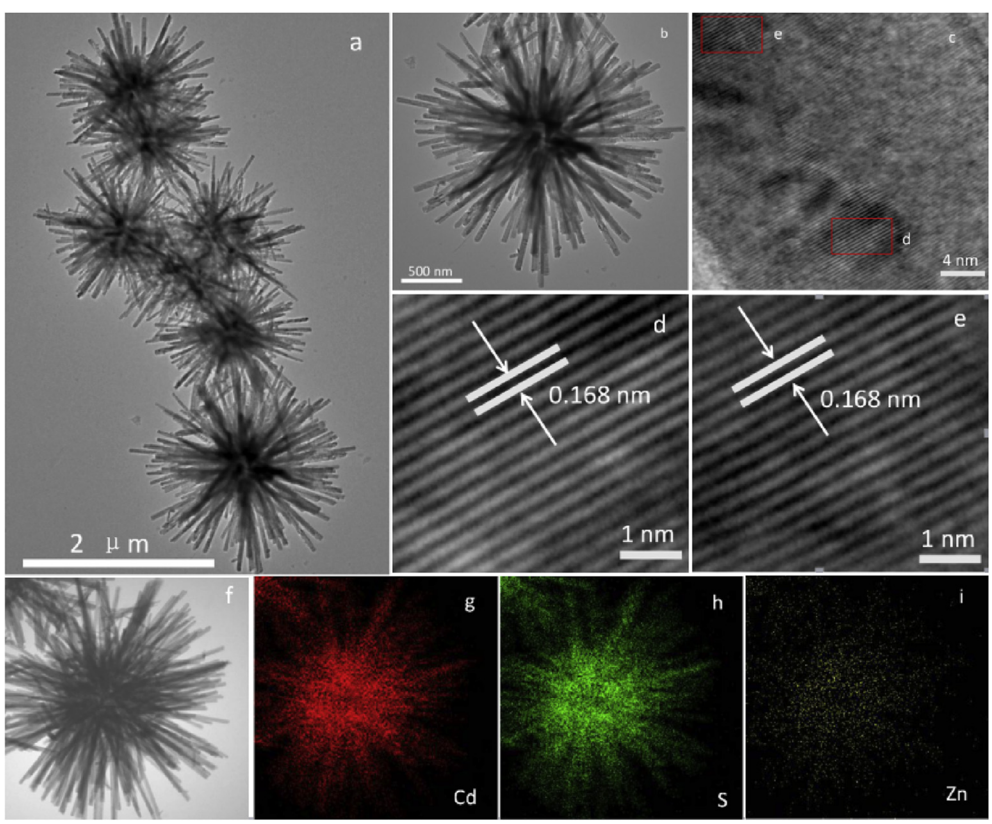

Fig. 3. (a, b, f) TEM images patterns of Zn doped CdS (S1); (c, d, e) HRTEM images of selected areas; (g)–(i) EDS elemental maps.

shown in Fig. 3e suggest that a whole nanorod is single crystalline. The d spacing of 0.168 nm (Fig. 3d) can be matched to (004) planes of hexagonal wurtzite CdS. The high aspect ratio of the nanorods means that they predominately grow in ⟨001⟩ direction. The elemental mapping images (Fig. 3g–i) confirm the composition of as-synthesized materials and the spatial distribution of the elements. Obviously, the element distributions of Cd and S are coincident with urchin-like hierarchical shape. Zn can also be detected in the whole hierarchical structure in consistence with the result of XRD.

3.2. Gas sensing properties

In General, the performance of the gas sensor is working temperature dependent. The working temperature can significantly affects the states of chemisorbed oxygen ions absorbed on the surface, as well as the activity of surface chemical reaction and consequent sensing properties. Therefore, to evaluate the sensing performance, the optimal working temperature for gas sensor should be tested firstly [27–29]. Fig. 4 describes the gas responses to 100 ppm ethanol for the gas sensors based on pure and Zn doped CdS (S1) at various temperatures. The sensitivity increases with the testing temperature till 225 °C. Further increased temperature results in a decreased response. This phenomenal may be attributed to the balance between surface chemical reaction and surface absorption/desorption process. Though the surface chemical reaction reactivity can improve with the temperature, at high temperature the desorption prevails to the absorption and consequently less target gas molecules can take part in the surface chemical reaction. Therefore, the optimal operating temperature is 225 °C. Both the pure and Zn doped CdS sensors have the highest responses at 225 °C. The sensitivity of S1 is 4.2 times higher than that of pure CdS. To further explore the effect of Zn doping, more amount of ZnO should be added in the synthesis process. But ZnO microcrystallines were apt to precipitate, forming uneven mixture of CdS and ZnO. Thus, in order to change the concentration of Zn doped in the final products, not the amounts of ZnO but $Cd(NO_3)_2$ were adjusted. Different volume of 0.1M $Cd(NO_3)_2$ precursor (0.25 ml, 0.50 ml, 0.75 ml) was added in the hydrothermal reaction mixture, the prepared products are labeled as S1, S2 and S3 respectively. The more $Cd(NO_3)_2$ there is, the smaller ratio of Zn ions in the final products is. Fig. 5 indicates that the sensitivity increases with the added ZnO quantity. Among the three samples, S1 has the highest sensitivity. Thus S1 was representatively selected for further measurements.

Besides ethanol, responses to other typical VOCs, including acetone, methanol, formaldehyde, toluene were shown in Fig. 6. As seen from it, Zn doping could improve the sensitivity for all the five target gases. Enhancement factors for toluene, ethanol, acetone, methanol and formaldehyde were 6.5, 4.2, 2, 2, 2, respectively. Obviously, its responses to ethanol are larger than those toward other alkyl-carbon oxygen compounds. Zn doped CdS showed good selectivity toward ethanol against other target gas with similar chemical structure. Furthermore, Zn doped CdS has good sensitivity

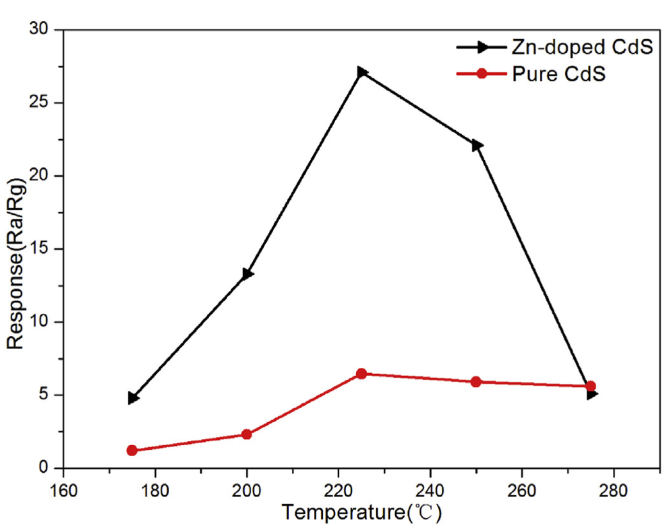

Fig. 4. Responses to 100 ppm ethanol for the gas sensors based on pure and Zn doped CdS (S1) at various temperatures.

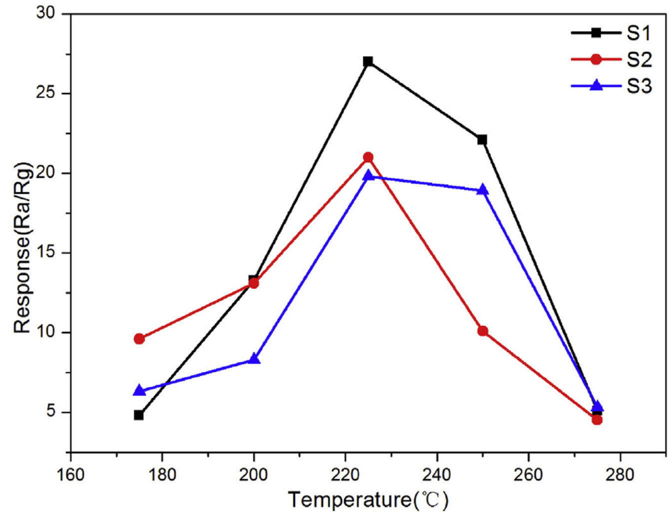

Fig. 5. Responses of the as-fabricated three gas sensors (S1, S2, S3) to 100 ppm ethanol as a function of operating temperature.

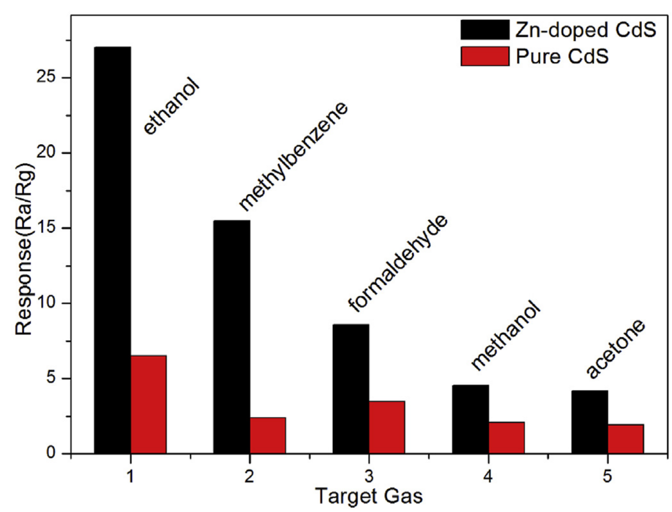

Fig. 6. Responses of pure and Zn doped CdS sample towards various gas (100 ppm) at 225 °C.

of 15 toward 100 ppm toluene. The response/recovery behavior of a sensor is a vital parameter in practical applications, especially in online monitoring systems. Fig. 7 exhibited the curves of dynamic response and recovery to 50 ppm ethanol at 225 °C for S1 sample. It displays extremely fast response and recovery, with the $\tau_{response}$ and $\tau_{recovery}$ of 1 and 8 s, respectively. This rapid response/recovery is beneficial to real-time monitoring for target gas. The response transients for various ethanol concentrations are presented in Fig. 8a. The sensitivity increased gradually with ethanol concentration (shown in Fig. 8b). In addition, upon increasing the ethanol concentration, the increasing rate of gas response improved. The reason for it is under investigation. Fig. 9 displayed 6 repetitive sensing transients to 50 ppm ethanol at 225 °C for Zn doped CdS (S1), indicating that the sensor based Zn doped CdS had good repeatability.

3.3. Gas sensing mechanism

The sensing mechanism for CdS could be clarified by the widely

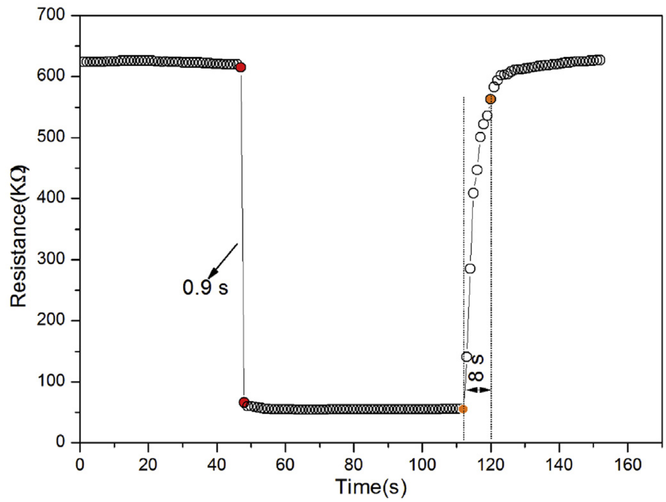

Fig. 7. Response and recovery curves t of the Zn doped CdS (S1)sensor to 50 ppm ethanol at 225 °C.

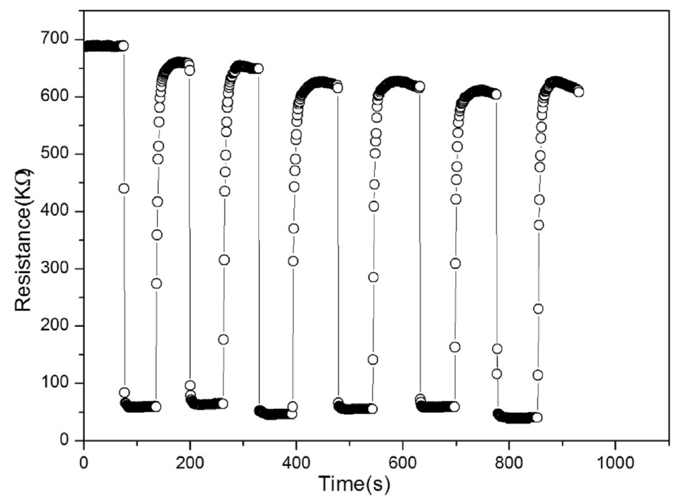

Fig. 9. Six repetitive transients to 50 ppm ethanol at 225 °C for Zn-doped CdS (S1).

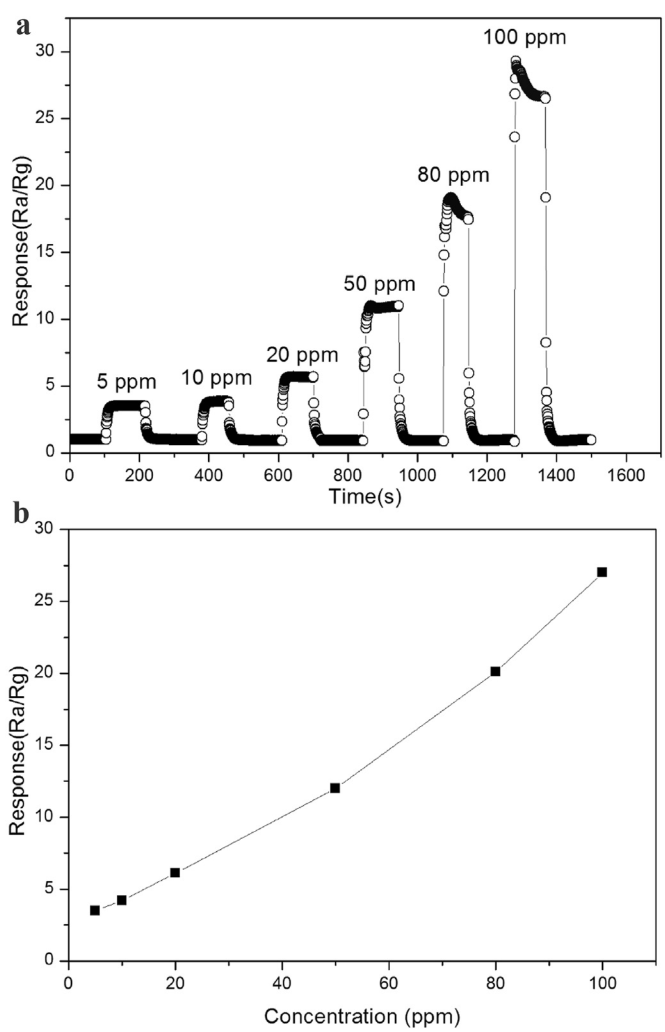

Fig. 8. (a) Dynamic response transients of Zn doped CdS sample to different concentrations of ethanol at 225 °C (b) Sensitivity (R_a/R_g) towards ethanol at various ethanol concentration.

accepted sensing theory for chemiresistive gas sensor. CdS is a typical n-type semiconductor with vacancy of S as donor. In the air, large amount of oxygen molecules can be adsorbed on the active sites at the surface of CdS. As a strong oxidant, absorbed oxygen molecules may capture free electrons from the conduction band of CdS to be transformed to chemisorbed oxygen ions, such as O_2^-, O^-, O^{2-}. Meanwhile, a depletion layer on the surface of CdS is formed, resulting in the increased resistance for CdS [30–32]. This progress can be expressed as the followings:

$$O_{2(gas)} \rightarrow O_{2(ads)} \tag{1}$$

$$O_{2(ads)} + e^- \rightarrow O^-_{2(ads)} \tag{2}$$

$$O^-_{2(ads)} + e^- \rightarrow 2O^-_{(ads)} \tag{3}$$

$$O^-_{(ads)} + e^- \rightarrow O^{2-}_{(ads)} \tag{4}$$

At the temperature of above 200 °C, $O^-_{(ads)}$ was believed to be dominant [33]. Upon exposure to reductive target gas, chemisorbed oxygen ions can oxidizing it, releasing electrons to the conduction band of CdS. These free electrons make depletion layer thin and the whole resistance of CdS decreased [34]. Taking ethanol gas as example, its reaction with chemisorbed oxygen ions is as follows:

$$C_2H_6O + 7O^-_{(ads)} \rightarrow 2CO_2 + 3H_2O + 7e^- \tag{5}$$

Zn doping can greatly enhance the sensing response to reductive gases. Carrier concentration may be one important factor for it. Due to the smaller radium of Zn^{2+}, Zn^{2+} doping can makes bond length short, as confirmed by the XRD results of Zn doped CdS. The short bond length means that valence strength is strong and the formation of S vacancy is getting difficult. Correspondingly, the concentration of S vacancy, which acts as donor, is decreased. As suggested by Kim etc [35], the low carrier concentration suggests that high ratio of free carriers can take part in the surface reaction and high response to reductive gases can be obtained. However, enhancement factors for different tested gas are different. Particularly, the responses to ethanol and toluene markedly increase with Zn doping. This supposes that not only carrier concentration but also surface activity are main factors for the improvement of the sensitivity.

4. Conclusions

In summary, unique and well-dispersed 3D urchin-like hierarchical CdS powders were synthesized via a simple one-step hydrothermal route. The performance of the gas sensors indicated Zn doped CdS-based sensor exhibited remarkable response and fast response-recovery speed to ethanol and toluene. The decreased carrier concentration and increased surface activity may the main factors for the improved sensing properties. The excellent sensing performance makes urchin-like hierarchical Zn doped CdS a potential sensing material.

Acknowledgments

This work is supported by National Key Research and Development Program of China (No. 2016YFC0201002). National Nature Science Foundation of China (Nos. 61503148, 61520106003, 61327804, 61374218) and Program for Chang Jiang Scholars and Innovative Research Team in University (No. IRT13018). National High-Tech Research and Development Program of China (863 Program, Nos. 2013AA030902 and 2014AA06A505). Science and Technology Development Program of Jilin Province (No. 20170520162JH). China Postdoctoral Science Foundation funded project No. 2015M580247.

References

[1] K.M. Li, Y.J. Li, M.Y. Lu, C.I. Kuo, L.J. Chen, Direct conversion of single-layer SnO nanoplates to multi-layer SnO_2 nanoplates with enhanced ethanol sensing properties, Adv. Funct. Mater. 19 (2009) 2453–2456.

[2] P. Sun, Y. Cao, J. Liu, Y.F. Sun, J. Ma, G.Y. Lu, Dispersive SnO_2 nanosheets: hydro-thermal synthesis and gas-sensing properties, Sens. Actuators B:Chem. 156 (2011) 779–783.

[3] F.H. Zhang, H.Q. Yang, X.L. Xie, L. Li, L.H. Zhang, J. Yu, H. Zhao, B. Liu, Controlled synthesis and gas-sensing properties of hollow sea urchin-like α-Fe_2O_3 nanostructures and α-Fe_2O_3 nanocubes, Sens. Actuators B:Chem. 141 (2009) 381–389.

[4] W. Yan, H.Q. Fan, Y.C. Zhai, C. Yang, P.R. Ren, L.M. Huang, Low temperature solution-based synthesis of porous flower-like α-Fe_2O_3 super structures and their excellent gas-sensing properties, Sens. Actuators, B 160 (2011) 1372–1379.

[5] C. Wang, J.Y. Liu, Q.Y. Yang, P. Sun, Y. Gao, F.M. Liu, J. Zheng, G.Y. Lu, Ultrasensitive and low detection limit of acetone gas sensor based on W-doped NiO hierarchical nanostructure, Sens. Actuators, B 220 (2015) 59–67.

[6] S. Elouali, L.G. Bloor, R. Binions, I.P. Parkin, C.J. Carmalt, J.A. Darr, Gas sensing with nano-indium oxides (In_2O_3) prepared via continuous hydrothermal flow synthesis, Langmuir 28 (2012) 1879–1885.

[7] P. Sun, C. Wang, X. Zhou, P.F. Cheng, K. Shimanoe, G.Y. Lu, N. Yamazoe, Cu-doped α-Fe_2O_3 hierarchical microcubes: synthesis and gas sensing properties, Sens. Actuators, B 193 (2014) 616–622.

[8] H.Y. Lai, T.H. Chen, C.H. Chen, Architecture controlled synthesis of flower-like In_2O_3 nanobundles with significantly enhanced ultraviolet scattering and ethanol sensing, CrystEngComm 14 (2012) 5589–5595.

[9] D.L. Chen, L.F. Ge, L. Yin, H.Y. Shi, D.W. Yang, J. Yang, R. Zhang, G.S. Shao, Solvent-regulated solvothermal synthesis and morphology-dependent gas-sensing performance of low-dimensional tungsten oxide nanocrystals, Sens. Actuators B Chem. 205 (2014) 391–400.

[10] J. Li, H.Q. Fan, X.H. Jia, Multilayered ZnO nanosheets with 3D porous architectures: synthesis and gas sensing application, J. Phys. Chem. C 114 (2010) 14684–14691.

[11] H.N. Hieu, N.M. Vuong, H. Jung, D.M. Jang, D. Kim, H. Kim, S.-K. Hong, Optimization of a zinc oxide urchin-like structure for high-performance gas sensing, J. Mater. Chem. 22 (2012) 1127–1134.

[12] D.W. Wang, S.S. Du, X. Zhou, B. Wang, J. Ma, P. Sun, Y.F. Sun, G.Y. Lu, Template-free synthesis and gas sensing properties of hierarchical hollow ZnO microspheres, CrystEngComm 15 (2013) 7438–7442.

[13] P. Sun, W.N. Wang, Y.P. Liu, Y.F. Sun, J. Ma, G.Y. Lu, Hydrothermal synthesis of 3D urchin-like α-Fe_2O_3 nanostructure for gas sensor, Sens. Actuators, B 173 (2012) 52–57.

[14] X.W. Li, J.Y. Liu, H. Guo, X. Zhou, C. Wang, P. Sun, X.L. Hu, G.Y. Lu, Au@In_2O_3 core–shell composites: a metal-semiconductor heterostructure for gas sensing, RSC Adv. 5 (2015) 545–551.

[15] X.X. Xu, X.D. Mei, P.L. Zhao, P. Sun, Y.F. Sun, X.L. Hu, G.Y. Lu, One-step synthesis and gas sensing characteristics of urchin-like In_2O_3, Sens. Actuators B Chem. 186 (2013) 61–66.

[16] R. Huang, X.J. Xu, C.P. Gu, M. Yang, M. Yang, J.H. Liu, Large-scale synthesis of hydrated tungsten oxide 3D architectures by a simple chemical solution route and their gas-sensing properties, J. Mater. Chem. 21 (2011) 13283–13289.

[17] C. Wang, R.Z. Sun, X. Li, Y.F. Sun, P. Sun, F.M. Liu, G.Y. Lu, Hierarchical flower-like WO_3 nanostructures and their gas sensing properties, Sens. Actuators B: Chem. 204 (2014) 224–230.

[18] D.L. Chen, L. Yin, L.F. Ge, B.B. Fan, R. Zhang, J. Sun, G.S. Shao, Low-temperature and highly selective NO-sensing performance of WO_3 nanoplates decorated with silver nanoparticles, Sens. Actuators B Chem. 185 (2013) 445–455.

[19] D.L. Chen, X.X. Hou, H.J. Wen, Y. Wang, H.L. Wang, X.J. Li, R. Zhang, H.X. Lu, H.L. Xu, S.K. Guan, J. Sun, L. Gao, The enhanced alcohol-sensing response of ultrathin WO_3 nanoplates, Nanotechnology 21 (2010) 035501–035512.

[20] P. Sun, X.D. Mei, Y.X. Cai, J. Ma, Y.F. Sun, X.S. Liang, F.M. Liu, G.Y. Lu, Synthesis and gas sensing properties of hierarchical SnO_2 nanostructures, Sens. Actuators B:Chem. 187 (2013) 301–307.

[21] C.P. Gu, X.J. Xu, J.R. Huang, W.Z. Wang, Y.F. Sun, J.H. Liu, Porous flower-like SnO_2 nanostructures as sensitive gas sensors for volatile organic compounds detection, Sens. Actuators B Chem. 174 (2012) 31–38.

[22] W.D. Shi, L.H. Huo, H.S. Wang, H.J. Zhang, J.H. Yang, P.H. Wei, Hydrothermal growth and gas sensing property of flower-shaped SnS_2 nanostructures, Nanotechnology 17 (2006) 2918–2924.

[23] X.Q. Fu, J.Y. Liu, Y.T. Wan, X.M. Zhang, F.L. Meng, J.H. Liu, Preparation of a leaf-like CdS micro-/nanostructure and its enhanced gas-sensing properties for detecting volatile organic compounds, J. Mater. Chem. 22 (2012) 17782–17791.

[24] L. Zhu, C.H. Feng, F. Li, D.Z. Zhang, C. Li, Y. Wang, Y. Lin, S.P. Ruan, Z.G. Chen, Excellent gas sensing and optical properties of single-crystalline cadmium sulfide nanowires, RSC Adv. 4 (2014) 61691–61697.

[25] L.H. Zhu, Y. Wang, D.Z. Zhang, C. Li, D.M. Sun, S.P. Wen, Y. Chen, S.P. Ruan, Gas sensors based on metal sulfide Zn1−xCdxS nanowires with excellent performance, ACS Appl. Mater. Interfaces (2015) 20793–20800.

[26] L.L. Zhang, H. Wang, W. Guo, J.M. Ma, Sensitive NO sensor based CdS microparticles assembled by nanoparticles, RSC Adv. 6 (2016) 45386–45391.

[27] X. Zhou, B.Q. Wang, H.B. Sun, C. Wang, P. Sun, X.W. Li, X.L. Hu, G.Y. Lu, Template-free synthesis of hierarchical $ZnFe_2O_4$ yolk–shell microspheres for high-sensitivity acetone sensors, Nanoscale 8 (2016) 5446–5453.

[28] V.R. Shinde, T.P. Gujar, C.D. Lokhande, Enhanced response of porous ZnO nanobeads towards LPG: effect of Pd sensitization, Sens. Actuators B 123 (2007) 701–706.

[29] Z. Cao, J.R. Stetter, A selective solid-state gas sensor for halogenated hydrocarbons, Sens. Actuators B 1–4 (1991) 109–113.

[30] X. Zhou, W. Feng, C. Wang, X.L. Hu, X.W. Li, P. Sun, K. Shimanoe, N. Yamazoe, G.Y. Lu, Porous ZnO/$ZnCo_2O_4$ hollow spheres: synthesis characterization, and applications in gas sensing, J. Mater. Chem. A 2 (2014) 17683–17690.

[31] X.W. Li, P. Sun, T.L. Yang, J. Zhao, Z.Y. Wang, W.N. Wang, Y.P. Liu, G.Y. Lu, Y. Du, Template-free microwave-assisted synthesis of ZnO hollow microspheres and their application in gas sensing, CrystEngComm 15 (2013) 2949–2955.

[32] N. Yamazoe, New approaches for improving semiconductor gas sensors, Sens. Actuators, B 5 (1991) 7–19.

[33] N. Barsan, M. Schweizer-Berberich, W. Gopel, Fundamental and practical aspects in the design of nanoscaled SnO_2 gas sensors: a status report, Fresenius' J. Anal. Chem. 365 (1999) 287–304.

[34] X. Xue, Z. Chen, C. Ma, L. Xing, Y. Chen, Y. Wang, T. Wang, One-step synthesis and gas-sensing characteristics of uniformly loaded Pt@SnO_2 nanorods, J. Phys. Chem. C 114 (2010) 3968–3972.

[35] H.J. Kim, Kwon-Il Choi, Kang-Min Kim,Highly sensitive C_2H_5OH sensors using Fe-doped NiO hollow spheres, Sens. Actuators B 171–172 (2012) 1029–1037.